FERMILAB-PUB-17-222-TD
ACCEPTED

Development of Low Angle Grain Boundaries in Lightly Deformed Superconducting Niobium and their influence on Hydride Distribution and Flux Perturbation

Z-H Sung[1], M. Wang[2], A. A. Polyanskii[1], C. Santosh[1], S Balachandran[1], C. Compton[3], D. C. Larbalestier[1], T. R. Bieler[2], and P. J. Lee[1]

[1]National High Magnetic Field Laboratory-Applied Superconductivity Center, 2031 E. Paul Dirac Dr., Tallahassee, FL, 32310, USA

[2]Mechanical Engineering, College of Engineering, Michigan State University, 428 S. Shaw Lane, East Lansing, MI, 48824, USA

[3]Facility for Rare Isotope Beams, Michigan State University, 640 South Shaw Lane, East Lansing, MI, 48824, USA

ABSTRACT: This study shows that low angle grain boundaries (LAGBs) can be created by small 5% strains in high purity (RRR ≥ 200) SRF-grade single crystalline niobium (Nb) and that these boundaries act as hydrogen traps as indicated by the distribution of niobium hydrides ($Nb_{1-x}H_x$). $Nb_{1-x}H_x$ is detrimental to superconducting radio frequency (SRF) Nb cavities due to its normal conducting properties at cavity operating temperatures. By designing a single crystal tensile sample extracted from a large grain (>5 cm) Nb ingot slice for preferred slip on one slip plane, LAGBs and dense dislocation boundaries developed. With chemical surface treatments following standard SRF cavity fabrication practice, $Nb_{1-x}H_x$ phases were densely precipitated at the LAGBs upon cryogenic cooling (8-10 K/min). Micro-crystallographic analysis confirmed heterogeneous hydride precipitation, which included significant hydrogen atom accumulation in LAGBs. Magneto-optical imaging (MOI) analysis showed that these sites can then act as sites for both premature flux penetration and eventually flux trapping. However, this hydrogen related degradation at LAGBs did not completely disappear even after a 800°C/2hrs anneal typically used for hydrogen removal in SRF Nb cavities. These findings suggest that hydride precipitation at a LAGB is facilitated by a non-equilibrium concentration of vacancy-hydrogen (H) complexes aided by mechanical deformation and the hydride phase interferes with the recovery process under 800°C annealing.

1. INTRODUCTION

Niobium (Nb) is the most well developed material for the fabrication of superconducting radio frequency (RF) cavities, which are the enabling core structures of linear particle accelerator such as SNS, CEBAF, FRIB, and Project X [1, 2]. The advantages of Nb derive from both its superconducting and mechanical properties. It has a relatively high lower critical field (H_{c1}), which allows RF magnetic fields up to 180-200 mT at 2 K [3], and is very ductile, which makes it easy to fabricate cavity shapes by a variety of techniques [1]. Achieving high accelerating gradients with a constant high quality factor, Q_0, (a measure of energy efficiency) while increasing accelerating fields ($H_{RF} \approx$ 120-150 mT) is a major goal for SRF cavity research. RF performance degradation, commonly known as 'Q-disease' and 'high field Q slope (HFQS)' are strongly related to surface contamination by oxygen (O) and hydrogen (H) [1,4-8]. The presence of surface oxides and hydrides are inevitable with the final chemical treatment steps to produce a damage-free smooth surface after cavity shape fabrication. The two available surface treatments are electropolishing (EP) and buffered chemical polishing (BCP). The strong passivity of Nb leaves dense multilayers of oxide (Nb_2O_5-Nb_2O-NbO, ~2-3 nm thick) on the surface [9-11] and substantial uptake of hydrogen occurs in the bulk of SRF Nb during these chemical processes [4, 5].

* now at Fermi National Accelerator Laboratory, Technical Division, Kirk road and Pine Street, Batavia, IL, 60510, USA, email: zsung@fnal.gov

To reduce the aforementioned RF performance degradation, heat treatments in two different temperature ranges under ultrahigh vacuum ($\geq 10^{-6}$ Torr) condition, ~100-120 °C for 48 h ("mild bake") and 600 °C/10 h - 800 °C/2 h ("anneal"), are effective. The former is for HFQS and the latter for 'Q-disease'. These heat treatments lead to; a) modification of the oxide layers [12,13], b) reduction of hydrogen density from the bulk [14,7], and c) reduction in the defect density introduced by the cavity forming process [15]. Of the surface oxides, the pentoxide (Nb_2O_5) is thought to be mainly responsible for the thermal breakdown of RF superconductivity due to its insulating (dielectric) property [4,6], and the development of magnetic moments is also possible if there are oxygen vacancies [16]. During mild baking, the Nb_2O_5 layer decomposes and O diffuses into the Nb matrix so that the surface (~100 nm) is in the "dirty limit" condition [12]. However, an understanding of the influence of the mild bake thermal process on hydrogen and hydride formation and their effect on surface RF superconductivity is still not fully developed.

The ubiquitous presence, size, and high mobility of H leads to a Nb-H solid solution [17]. As the cavity is cooled down, the hydride phase ($Nb_{1-x}H_x$) precipitates from a super-saturated solution around 100-130 K [7,17,18]. Nb hydride leads to significant RF loss during the cavity operation since its critical superconducting temperature, T_c ~1.5 K, is lower than the cavity operation temperature of 2-4 K [6, 17]. Romanenko proposed that the 120 °C bake significantly reduces hydride formation and correspondingly indicated a sharp reduction in the dislocation density [7] as well as reduction in near surface vacancy-H complexes [19]. In the Romanenko model, it is suggested that vacancy-H complexes are preferential hydride precipitation sources, and the 120 °C bake reduces the numbers of vacancy complexes leading to dissociation of vacancy-H. Although the number of free H atoms are now increased they are not precipitated due to absence of favorable traps, and high hydrogen mobility in the Nb lattice. Elastic recoil detector experiments indicated that the hydrogen content does not vary with the range and time period of thermal treatments [20] and there may still remain the appearance of small size (< 100 nm) hydrides after heat treatments, which might be responsible for HFQS [20,21]. Using a cryogenic laser confocal microscope, Barkov [18,22] observed in-situ hydride formation on an SRF-grade Nb coupon whose surface was mechanically damaged with conventional mechanical polishing and chemical treated with BCP or EP. However, the hydride phase did not precipitate within the resolution of this technique (>~120 nm) after 120 °C/24 h bake or 800 °C/3 h anneal treatment. Kim [23] and Tao [24] investigated regions in the vicinity of 'hot spots' (the areas identified by thermometry during cavity testing), using atom probe tomography in conjunction with cryogenic scanning transmission electron microscopy. This atomic scale study showed that hot spot regions have high hydrogen content, and hydrogen atoms naturally accumulate at the interface between the surface oxide layer and the Nb metal matrix. This is consistent with the findings of secondary ion mass spectroscopy (SIMS) investigations [4, 25]. The dense Nb oxide phase is a protective layer that blocks transport of H into SRF Nb. This local enrichment of H atoms at the interface of Nb and Nb oxides leads to favorable conditions for hydride precipitation. Using cryogenic TEM, Trenikhina [26] also showed that the 120 °C bake can reduce the number of hydrides by ~40-50 % on an EP'ed cavity surface.

From these detailed studies, there is clear evidence of defect related hydride formation and RF performance improvement when "H" contamination is modified by thermal treatments. From a fundamental microstructure point of view, a determination of the interactions between commonly occurring defects and hydrogen is desirable in high purity Nb. The commonly occurring defects in bulk Nb that are relevant to changes in the surface superconducting properties are vacancies, dislocations, impurities, and low and high angle grain boundaries. Thus, understanding of the effect of plastic deformation of Nb on hydride precipitation is very relevant to development of better cavity processing techniques. Mechanical deformation for cavity shape fabrication causes dislocation multiplication [15], a non-equilibrium vacancy concentration [27], and formation of dense dislocation walls like planar grain boundaries or low angle grain boundaries (LAGBs) [28,29]. It is well known that the core of dislocations is of concern because an "H" rich site (Cottrell cloud) [7, 30] and vacancies also facilitate the formation of hydrides [19,20].

In this study, the dislocation content of a high purity SRF-grade Nb single crystal was increased in particular planes by applying 5% tensile strain to a selected single crystal SRF Nb coupon sample with a well

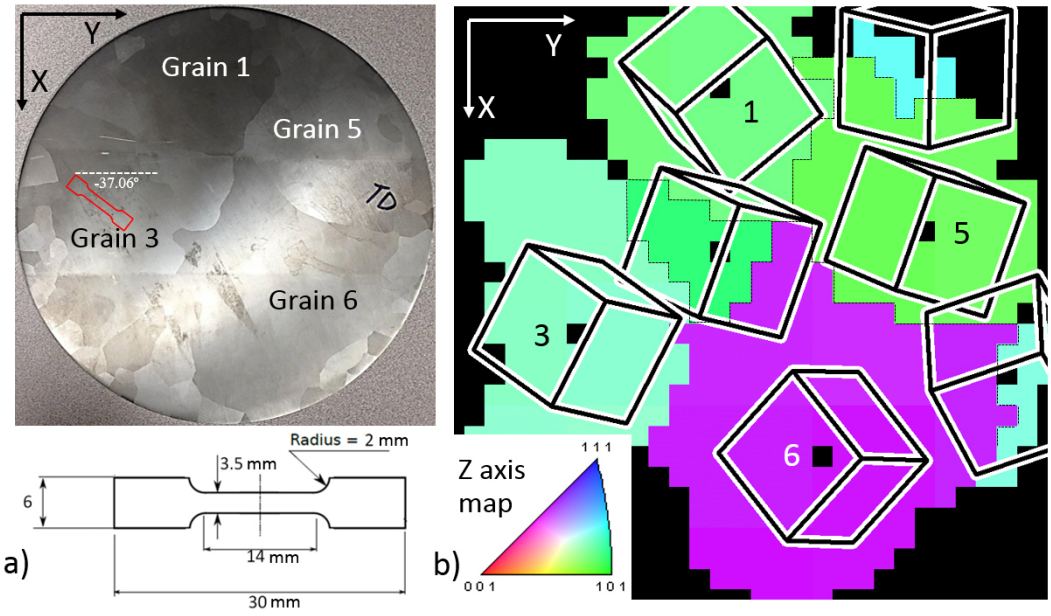

Figure 1. (a) (top) SRF-grade, high purity (RRR ≥ 200), large grain (> 5-10 cm), niobium ingot slice with a diameter of 270 mm and a thickness of 3 mm, manufactured by Tokyo Denkai and (bottom) the dimension of the tensile strain test coupon. The red outline represents the ~37.1° angular rotation of EDM extraction for the test coupons at Grain 3. (b) Grain crystallographic orientation normal to the slice surface, characterized with Laue X-ray diffraction and OrientExpress indexing program [32]. The inset shows the orientation color legend, and the unit cells indicate the crystal orientation of each grain.

characterized crystallographic orientation. The sample was then polished to provide a favorable environment for Nb hydride precipitation at planar defects such as dense dislocation walls or low angle grain boundaries (LAGBs). Magnetic flux behavior perturbed by local $Nb_{1-x}H_x$ segregation is evaluated using magneto-optical imaging (MOI) after the chemical treatment and a subsequent 800 °C heat treatment. The presences of Nb hydride formation is observed by comparing surface topological features before and after the cryogenic cooling. Defects that might be favorable for hydride segregation were investigated using transmission electron microscopy (TEM) and electron backscattered diffraction (EBSD). This study seeks to help clarify the relationships between plastic deformation induced dislocations and hydride precipitation and their effect on superconductivity of SRF Nb.

2. EXPERIMENTAL DETAIL

2.1. SELECTION OF THE SAMPLE

An SRF-grade, high purity (RRR: residual resistivity ratio ≥ 200), large grain (grain diameter > 50 mm), niobium ingot slice fabricated by Tokyo Denkai using multiple electron beam melting (EBM) [31] was provided by FRIB for this study. The left optical image in Figure 1 shows an overview of this Nb ingot slice, having ~10 single grains at the center and ~30 small grains along the circumference, with a diameter of 270 mm and a thickness of 3 mm. Surface normal orientations of the seven largest single grains were characterized by Laue X-ray diffraction and indexed using OrientExpress software [32]. The right color map in Figure 1 shows the obtained crystal orientations and the cubic lattices orientation for each grain, based upon defining the Y axis as horizontal and Z out of the page.

The Schmid factor describes the likelihood of activating a slip system based upon uniaxial deformation and the crystal orientation. For uniaxial deformation, the value of the Schmid factor is between 0 and 0.5 (where 0.5 represents a soft orientation where the resolved shear stress on a slip system is as high as it can be) [14]. The direction of tensile strain was chosen to maximize activation of slip on a {112} plane. Using a MATLAB code [32,33], the Schmid factors were computed based on the measured grain orientation (Bunge Euler angles φ_1, Φ, φ_2 = 167° 141° 108°). Figure 2 shows all possible Schmid factors for each of the 24 slip systems as a function of the first Euler angle. A rotation of the sample by 37.1° or rotating the tensile sample orientation 37.1°

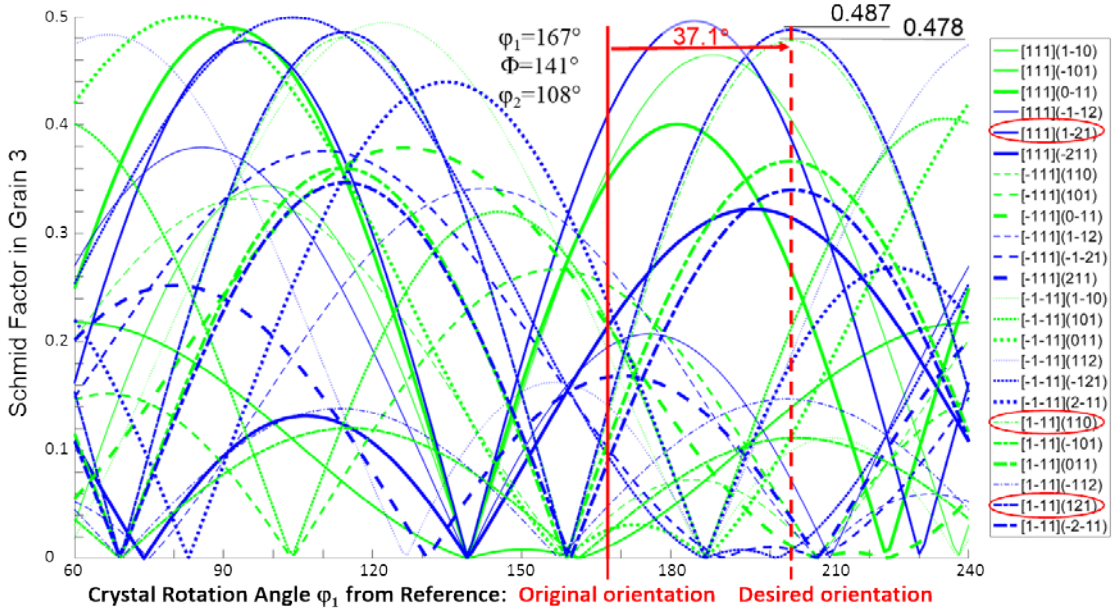

Figure 2. Absolute value of Schmid factor calculated for all slip systems in grain # 3 (Figure 1) with the red solid line representing the reference orientation and the dashed line indicating the desired orientation to favor $[1\bar{1}1]$ slip system on (121) and (101) plane.

gives the $[1\bar{1}1]$ (121) and the $[1\bar{1}1]$ (110) slip systems their maximum Schmid factor (dashed red line). Thus, the sample was extracted using electrical discharge machining (EDM) with this extra 37.1° rotation, as illustrated in Figure 1a.

The tensile sample was uni-axially strained to reach a level of 5 % strain. For magneto-optical imaging (MOI) analysis, each deformed sample was cut into four small pieces (3 × 3 × 1.5 mm), making tilted cuts to align dislocation Burgers vectors to be parallel or perpendicular to the sectioned surface (not shown in Figure 3). The tilted cuts were determined so that the slip plane was parallel to the cut surface for the "left" samples (c & d), and so that the "right" samples (a & b) have the slip plane perpendicular to the surface. Thus, the dislocation Burgers vectors are perpendicular in these two different types of the sample surfaces. As screw dislocations are expected to predominate (due to their lower mobility than edge dislocations) then both edge and screw line directions are parallel to the surface in the "left" slices (c & d), and screw dislocations are perpendicular to the surface in the "right" slices (a & b). Thus, these samples were designed to examine how the magnetic field would interact with screw dislocations perpendicular to the magnetic field (left) or parallel to the magnetic field (right).

2.2. MAGNETO-OPTICAL IMAGING (MOI)

Magneto optical imaging (MOI) uses the strong Faraday effect in bismuth doped yttrium iron garnet (B-YIG) to measure the change of the vertical magnetic field component (H_z) above a superconducting sample using a standard polarized light microscope. The technique is able to resolve fields of the order of 1 mT with ~5–10 μm spatial resolution [34]. Three different MOI operation modes, ZFC (Zero Field Cooled), RF (Remnant Fielded), and FC (Field Cooled), were used to observe the local redistribution of the magnetic flux in these coupons, when cooled below the T_c of Nb ~9.2 K. ZFC MO imaging shows perturbation of the surface superconducting properties on the sample after cooling well below T_c and then applying an increasing external magnetic field until the sample is fully penetrated. For RF mode the procedure for ZFC is followed, but after the sample is significantly penetrated, the external magnetic field is removed so that magnitude and distribution of the remnant magnetic flux can be obtained. For FC mode MO imaging, the sample is cooled below T_c while in the presence of an externally applied magnetic field and then the external field is removed; this mode is more sensitive to the bulk superconducting properties because the field was fully penetrated. In this FC mode, normal conducting artifacts such as bulk defects, impurities, and grain boundaries

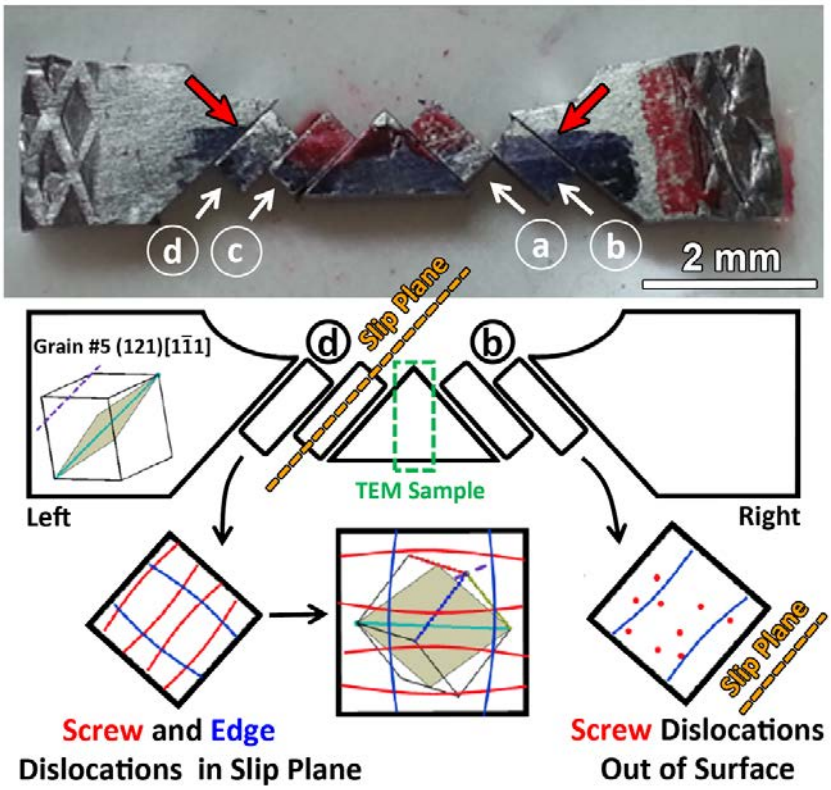

Figure 3. [Top] Optical image of the test coupon of single grain #3 (Figure 1) after 5% tensile strain deformation and EDM sectioning (sample ID of four small pieces: a to d). The red arrows indicate the direction of magneto-optical (MO) imaging, which is the opposite direction of the externally applied magnetic field during MOI. [Bottom] A schematic diagram showing the estimated direction of the slip plane and the anticipated screw and edge dislocation morphology in a MOI viewing plane. The unit cell illustrates the gray (121) slip plane and the blue [1$\bar{1}$1] slip direction vector (screw line direction). In the left sample (c & d), edge and screw dislocation lines are parallel to the MOI viewing plane (slip plane); in the right sample (a & b), screw dislocation lines are perpendicular to the MOI view direction.

are often visible as dark features because they are preferential routes for flux trapping. In this mode, a homogeneous defect-free square sample would exhibit a perfect "rooftop" pattern of diagonal bright lines crossing from the four corners.

2.3. MICROSTRUCTURE AND MICROCRYSTALLOGRAPHIC ANALYSIS

The microstructural properties of the selected 5% tensile deformed sample were characterized using a JEOL ARM 200F transmission electron microscope (TEM). TEM thin foils were prepared by slicing the remaining central part (triangle) of the deformed sample (Figure 3) with a precision diamond saw so that the TEM sample normal was parallel to the tensile strain direction. Sliced samples were initially mechanical thinned to ~150-200 µm thickness by diamond lapping and then subsequently reduced to ~80-100 µm in central thickness by a dimple grinder. To observe pristine cold-work deformed structure, thinned specimen were finalized for electron transparency using a Struers Tenupol-5 Twin-Jet polishing system with a solution of 6-8 vol.% H_2SO_4 in methanol. This electric jet polishing is preferred over the focused ion beam (FIB) technique in TEM sample preparation for observation of dislocation morphology in soft metals like Nb because the heavy Ga ions of the FIB can easily disturb the lattice structures of the soft metal surface, which leaves point defects on the TEM sample surface. Electron backscattered diffraction (EBSD) - orientation imaging microscopy (OIM) was used to characterize the micro-crystallographic features on the sample surface. The OIM was performed in a Zeiss 1540 EsB field emission scanning electron microscope (FESEM) equipped with an EDAX-Hikari high speed OIM camera. Using a 15 keV electron beam energy, we were able to scan the surface with a small (50-100 nm) step size which can

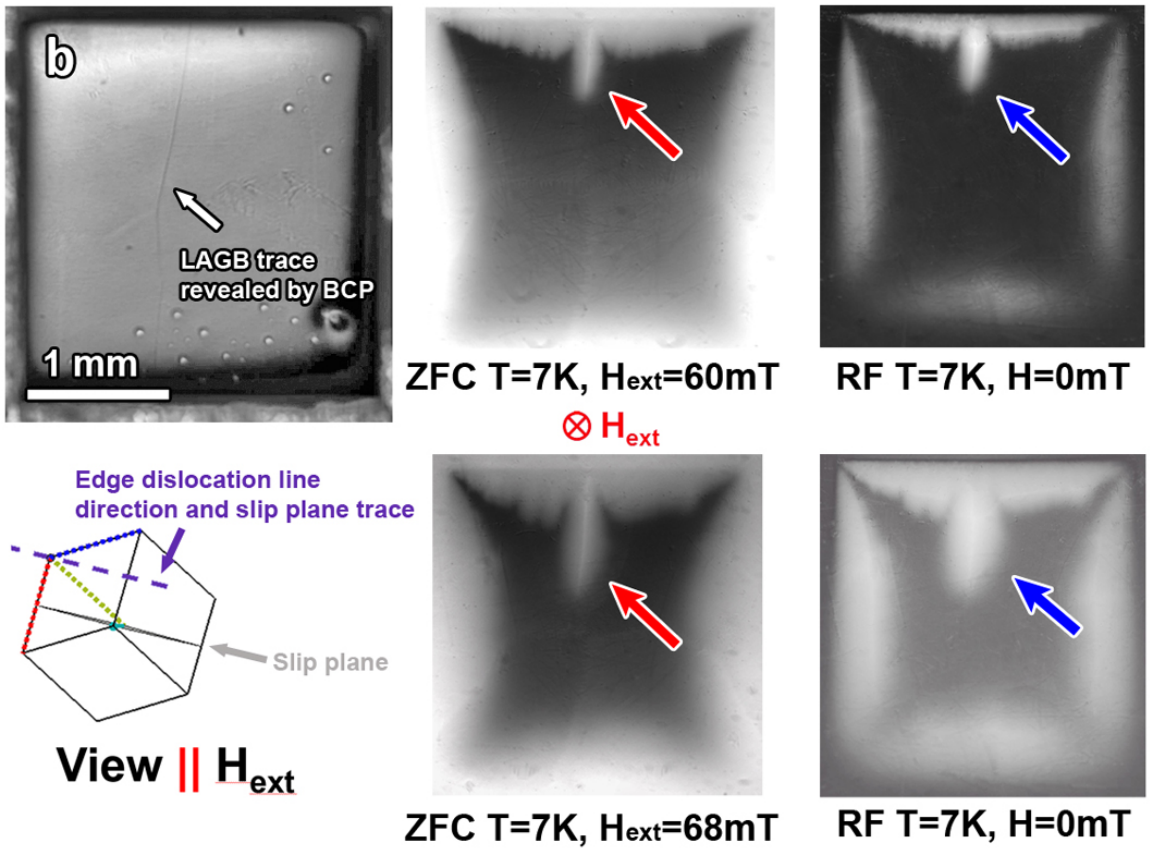

Figure 4. ZFC and RF mode MO images of the "right" sample (b, Figure 3) with the orientation of the slip plane (perpendicular to page) with screw dislocation lines out of the viewing plane/slip plane and the edge directions line direction indicated by the violet dotted line.

identify the crystallographic orientation at a sub-micrometer-scale with a precision of better than 0.1 degree.

3. RESULTS

The 30 minute BCP revealed low angle grain boundaries (LAGBs: <1-5 degree) on the gently polished single crystal Nb samples, as shown in the optical images (top left) in Figure 4 and Figure 5, which have either screw dislocation lines out or in the viewing plane, respectively. These LAGBs were apparently produced during the 5 % tensile strain cold work deformation. Chemical polishing produced grooves at LAGBs that are similar to those typically produced at high angle grain boundaries (HAGBs > 15 degree). ZFC and RF mode MO images in Figure 4 and Figure 5 show magnetic flux behavior on the samples below the 9.2 K T_c of Nb. During MO imaging, external magnetic fields were applied normal to the sample surface, so that the activated dislocation slip plane was aligned parallel to the direction of the magnetic field. The external magnetic flux clearly penetrates into the LAGBs earlier than into the grains, as indicated by the red arrows in both images. Likewise, RF MO images show distinct contrast variations at LAGBs, as indicated by the blue arrows, which implies significant disturbance of circulating superconducting currents at LAGBs.

However, not all LAGBs are responsible for this magnetic flux perturbation. Flux penetration occurs only on the upper part of the LAGB in Figure 4, and only some LAGBs are involved in the flux penetration, as indicated by the blue and green dotted lines in Figure 5. In addition, no distinguishable difference is found with regards to dislocation morphology. Since the cooling temperature and magnetic field were carefully chosen for optimum monochromatic contrasts for MO imaging, the difference in the amount of penetration from the edges between two samples might not directly implicate any difference in superconducting properties.

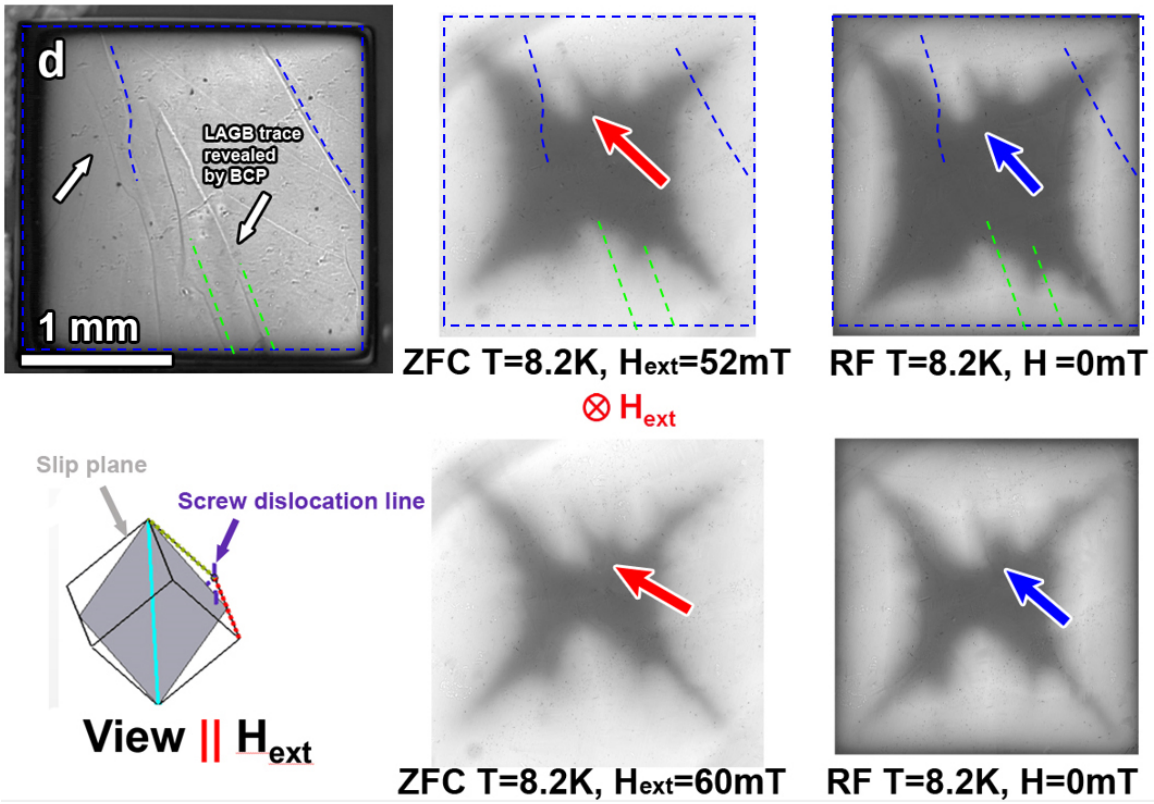

Figure 5. ZFC and RF mode MO images for the "left" sample (d, Figure 3); the configuration of the gray (121) slip lane and the screw dislocation line direction (violet dotted line and teal line) screw dislocation line direction is in the viewing plane/slip plane. In the upper images, small offset blue and green dotted lines are applied for easy recognition of the GB locations.

Bright field (BF) transmission electron microscope (TEM) images in Figure 6 show the microstructure of the 5% deformed Nb samples having cell structures with dense dislocations walls. The cell block structure is typical of a metal with medium to high stacking fault energy after plastic deformation [35]. A high density of dislocation networks is observed in planar boundaries, as indicated by the red arrows. These boundaries are low angle grain boundaries (LAGBs) due to their low lattice misorientation angle (< 1-5 degree) between cell blocks.

The sketch depicting two dislocation sources on a (101) and a (121) plane on either side of a boundary shows how dislocation walls may develop between two sources. If they operate at unequal rates, the number of dislocations from each would lead to an accumulating misorientation. The inclination of dislocations walls would be 45° from the slip plane, as (nearly) opposite signed dislocations have stable positions that would lead to walls that are either parallel or perpendicular to the tensile axis, resulting in roughly square tubes of dislocation walls perpendicular to the Burgers vector and perpendicular to the tensile axis. A more detailed study is needed to precisely describe the dislocation substructure, but these images clearly show development of low angle boundaries consistent with Figure 4, Figure 5, and Figure 7.

To conduct the MOI analysis, the samples were cooled below the 9.2 K T_c of Nb at a rate of 8-10 K/min from ambient temperature under a ~10^{-2}-10^{-3} Torr vacuum. Figure 7 compares the surface morphological features of the samples before and after the cryogenic cooling. Many blister-like surface relief structures appeared on the surface after cooling. This topological change is consistent with the observation of a laser confocal microscopy study [18,22], and these structures are attributed to hydride precipitations that occurred between T ~100-130 K. The hydrides are believed to be stable during MOI, but after MOI, when the sample temperature is ramped back up above the saturation temperature, the hydrides decompose and leave residual scars on the surface. Most interestingly, the hydride

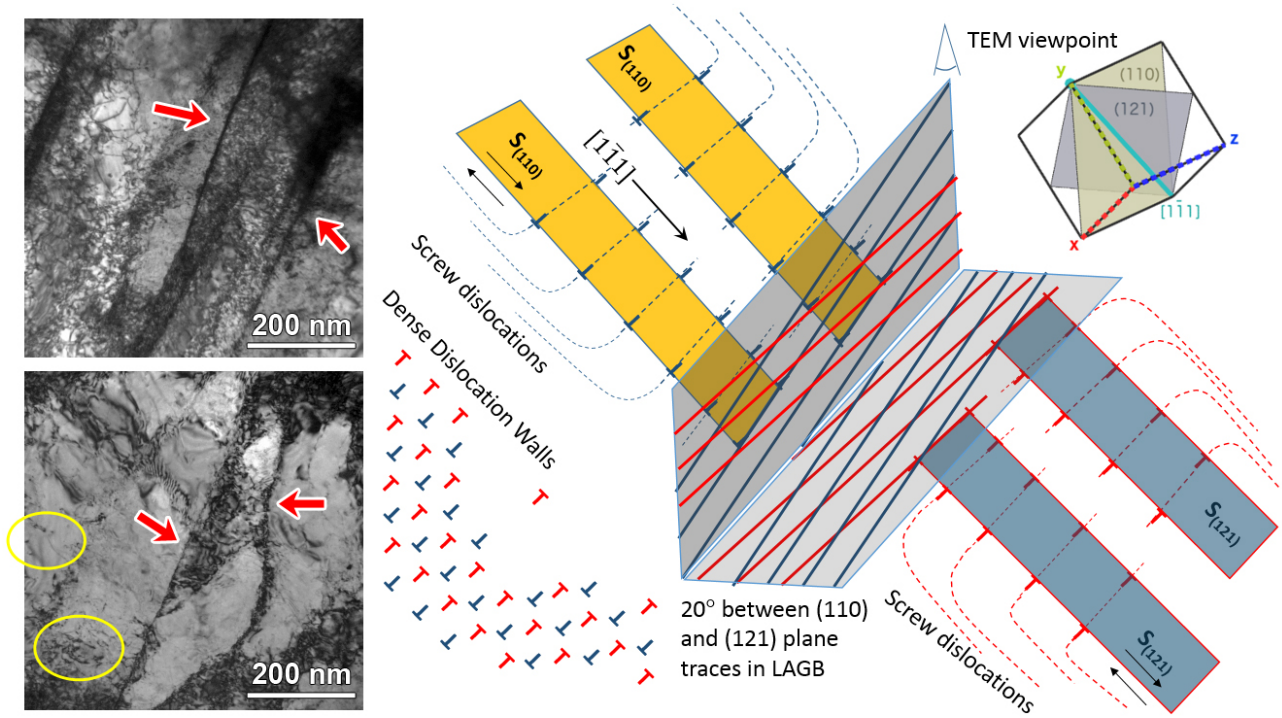

Figure 6. Bright field (BF) transmission electron microscope (TEM) images of cross sectional microstructure (normal to the tensile direction) of the 5% tensile strained grain # 3 (Figure 3), and a schematic of the possible dislocation arrangement on sub-boundaries parallel and perpendicular to the tensile axis.

phases preferentially precipitate along the LAGBs in this sample, as indicated by the surface topography. Even some LAGBs that had not previously been identified from surface grooving after BCP were revealed by hydride precipitation. These topological features are more easily observed in the enlarged area images (the rightmost) of Figure 7.

Micro-crystallographic structures at the vicinity of the LAGB where premature magnetic flux penetration occurred (Figure 5, "left" sample, d) was characterized using FESEM/EBSD-OIM. An FESEM secondary electron image (Figure 8b) shows further details of the hydride scars resulting from hydride segregation both along the LAGB and within the grains. Most interestingly, ~20-60 µm width of clean areas appeared at either side of the LAGB, as marked with the blue arrows, which suggests a strongly reduced hydride concentration or size in those areas. To investigate these features further, a local average misorientation map (Figure 8c) is reconstructed based on the EBSD scan [36]. The map shows that the hydride scars are misoriented by 5-9º from the surrounding crystal. This is also consistent with the fact that hydride precipitates form as islands on the sample surface [19]. There appear to be two distinct sizes of the hydride scars, a 1 µm size closer to the LAGB and 10 µm features more than 50 µm away from the LAGB. Near the LAGB, there is no evidence of hydrides within 10 µm to left of the LAGB and 50 µm to the right of the LAGB. The shapes of the hydride scars suggest an orientation sensitivity to the distribution of hydrogen or hydride precipitates.

A misorientation profile across a LAGB hydride scars is plotted in Figure 8c and shows the intrinsic crystallographic misorientation features related to the hydride scars that we have observed. This plot also shows that the LAGB offset is only about 1/2°, *i.e.* at the angular resolution limit of our EBSD analysis. At the bottom of the map, a nearly horizontal boundary also has hydrides decorating the line, but the angle of misorientation decreases from right to left, such that the boundary misorientation is apparently too low to support hydride nucleation close to the vertical boundary.

To determine the effect of the standardized cavity thermal treatment on "H" contamination at LAGBs, the small Nb samples were annealed at 800 °C for 2h under ultrahigh vacuum (10^{-6} Torr) after the first MO imaging

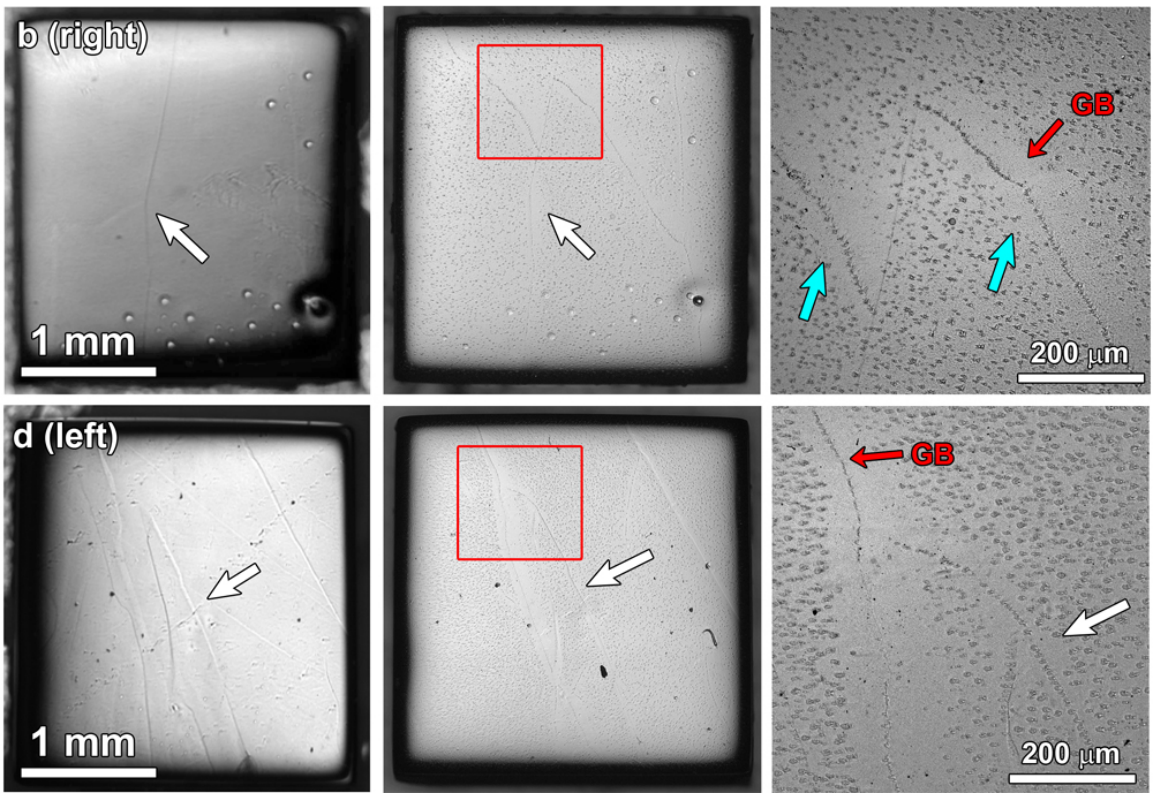

Figure 7. Surface optical images of the "right" sample (b, upper) and the "left" sample (d, lower) before (the leftmost) and after (the middle) cryogenic cooling below T_c of Nb ~9.2 K for MO imaging. The rightmost images that show enlarged areas in the vicinity of LAGBs, as indicated with red rectangles clearly show surface scar features resulting from hydride precipitation.

analysis, and then re-analyzed using MOI. It is empirically known that 600°C for 10h or 800°C for 2-3h anneal can expel most of the H atoms from the bulk of SRF Nb [14,22] and no additional micron sized hydride relief after temperature cycling of the annealed samples was observed. Figure 9 shows both ZFC and FC mode MO images of the two samples having different dislocation morphology (see Figure 3) after 800°C annealing. The flux penetration into the samples is not markedly different, although local penetration is observed, as indicated by the red arrows, and this penetration is coincidently associated with the same vertical LAGB in the left (d) and right (b) samples observed prior to heat treatment. They appear to initially penetrate from the top surface rather than the edges. The penetrated regions also appear broader and additional locations are observed. The FC mode images also show some contrast changes for trapped magnetic flux at the "weak" LAGBs, marked by the blue arrows. However, similar to the initial MO imaging, not all of entire LAGBs are responsible for the magnetic flux perturbations, as represented with the small offset blue and green dotted lines. Contrary to the first MOI, a clear rooftop pattern contrast appears on the surface. This rooftop pattern is created when strong superconducting currents circulate in the bulk of the material. These results suggest that the 800°C anneal likely recovered most of bulk properties affected by H contamination, but was not fully effective at the LAGBs.

4. DISCUSSION

With precise evaluation of grain crystallographic orientation for the maximum shear stress, we were able to successfully induce the formation of low angle grain boundaries (LAGBs) in a high purity SRF-grade single crystalline niobium by applying only a 5% tensile deformation. Through buffer chemical polishing (BCP) following with hydrofluoric acid (HF) rinsing, significant hydrogen upload was demonstrated to occur, leading to favorable environments for Nb hydride ($Nb_{1-x}H_x$) segregation. Surface topological and microstructural analysis confirmed the appearance of preferential hydride precipitation along the LAGBs upon cryogenic cooling. MO imaging suggests that this LAGB segregation could be a contributor to premature

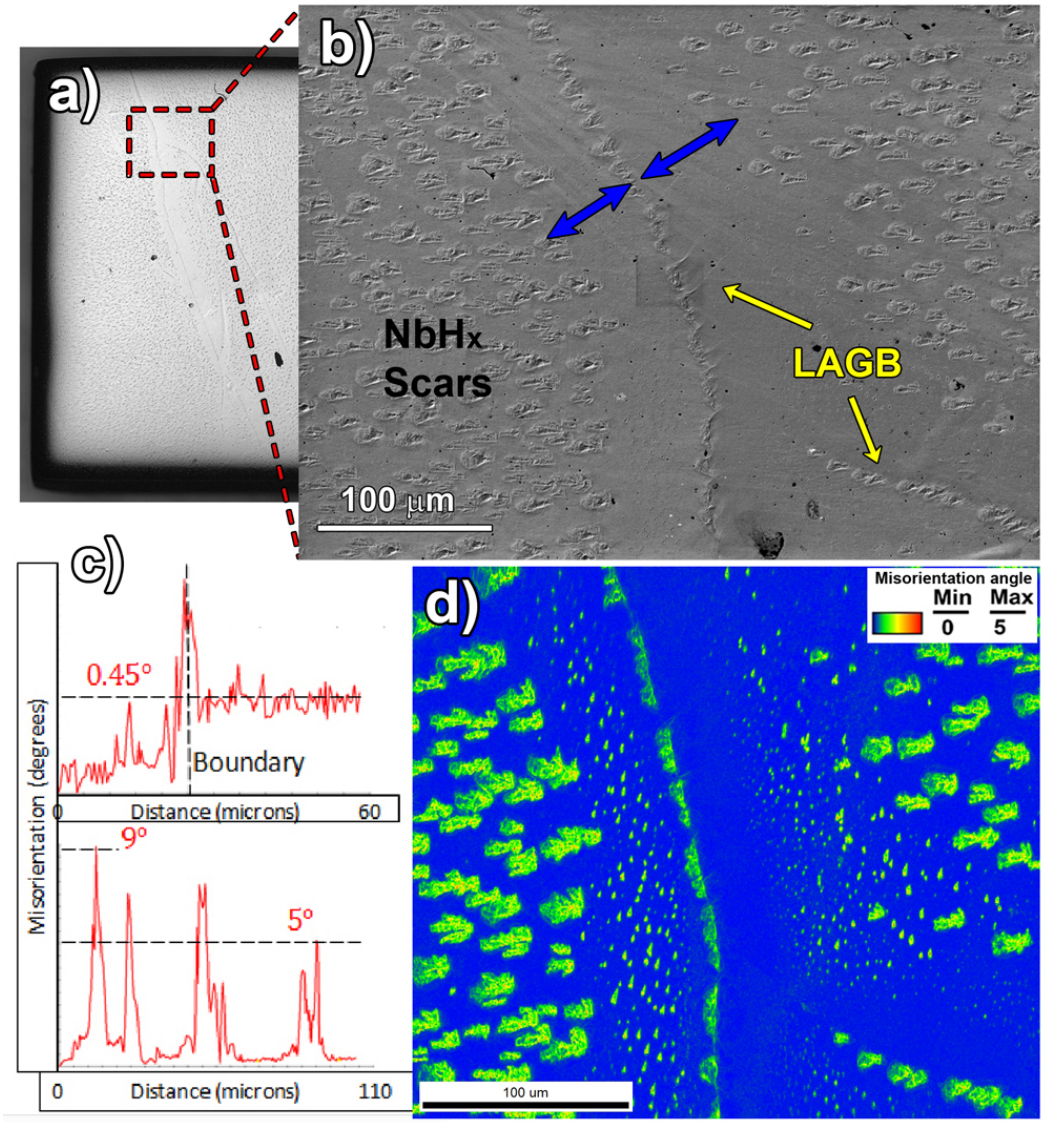

Figure 8. (a) Light microscopy image of the LAGB where premature magnetic flux penetration occurs in MOI analysis (Figure 5, the "left" sample, d) with (b) higher magnification scanning electron microscope secondary electron image of the area indicated by the dotted rectangle in the optical image, (d) local average misorientation map with misorientation profiles (c) along two line traces and through several hydride scars (top) and across the LAGB (bottom), from electron backscattered diffraction (EBSD) data.

magnetic flux penetration and magnetic flux trap, observed for some of the LAGBs. Subsequent annealing at 800°C/2h significantly changed the mode of flux perturbation but areas of weakness remained.

4.1. DEVELOPMENT OF LAGBS AT LOW TENSILE STRAIN IN NIOBIUM

The effect of strain on the microstructure of SRF Nb is important because mechanical deformation is used to form the cavity shapes and additional post-fabrication deformation is used to tune multi-cell cavities. Compared to other BCC metals, dislocations in pure Nb are stable because the interaction forces for driving dislocations in slip systems are small, and dislocation entanglements lead to much smaller internal stress [15]. Dislocation slip occurs when the resolved shear stress exceeds the critical resolved shear stress, which can be quantitatively estimated with Schmid factor [32]. In this study, a minimal cold work deformation of only 5% led to the formation of cell structure consisting of

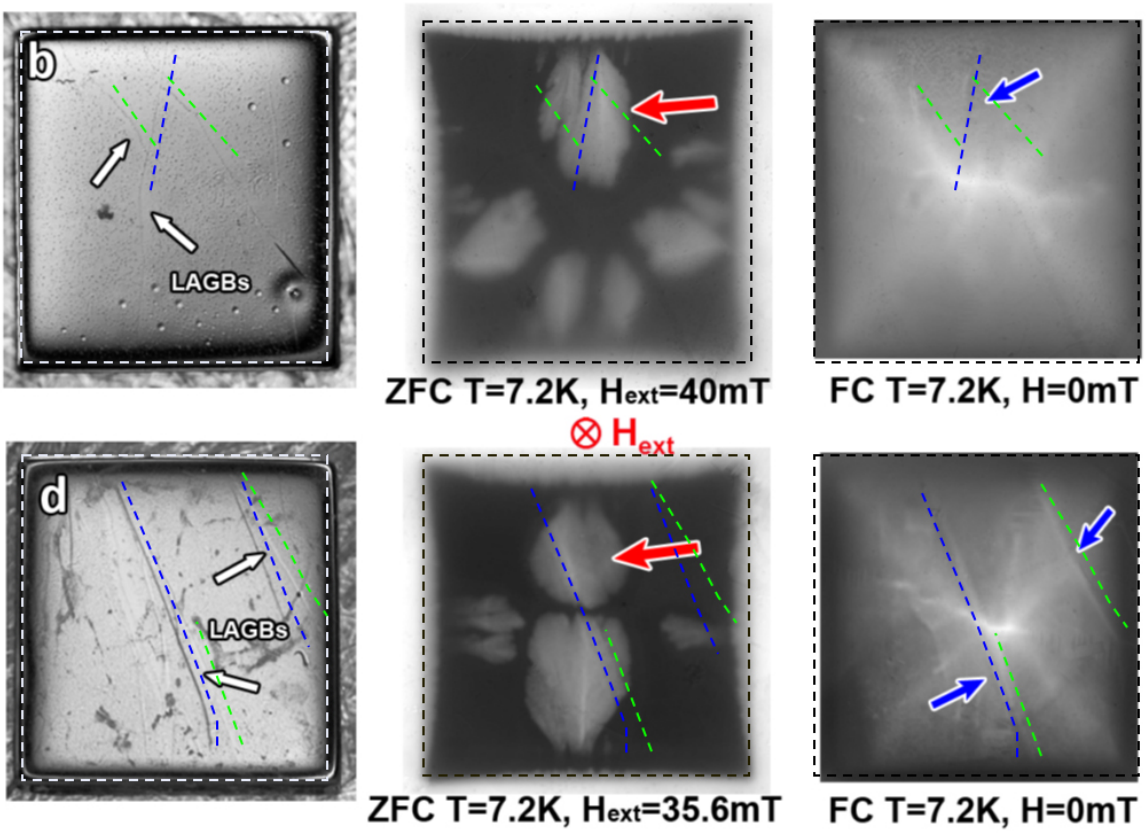

Figure 9. ZFC and FC mode MO images of the "right" (upper images, b) and "left" (lower images, d) samples after 800 °C/2hrs anneal under ultrahigh vacuum (≥ 10^{-6} Torr). Small offset blue and green dotted lines are applied for easy recognition of the GB locations.

dislocations, as shown in the BF TEM images of Figure 6.

In metallic deformation, such cell structures result from one of two mechanisms; dislocation accumulation between regions with different strain patterns or mutual trapping of dislocations into low energy configuration [28]. These two different systems induce two different boundary conditions, i.e., geometrical necessary boundaries (GNBs) or incidental dislocation boundaries (IDBs), respectively. Dislocation slip with different strain patterns accommodates the lattice orientation, so that GNBs show a higher misorientation angle across the cell blocks, compared to the IDBs [28,29]. To form these planar boundaries, external activation energy either by heat treatment or high cold work deformation (> 20%) is typically required to rearrange dislocations, especially in cavity grade Nb [33, 37]. However, this sample formed LAGBs with only 5% tensile deformation followed by BCP chemical treatment and hydride precipitates resulting from subsequent cryogenic cooling. Thus, it appears that preferentially activating one slip direction on two planes could lead to rearrangement of statistically stored dislocations into a low energy substructure as illustrated in Figure 6. Alternatively, pre-existing subgrain boundaries may have provided a site for accumulation of dislocations during the deformation. At this time, we cannot distinguish an already existing sub grain boundary from a newly created GNB during deformation from an analysis of misorientation angle [28]. It is also possible that Nb hydride phase formation or transformation during the cooling process might locally provide a driving force for creation of dislocation structure. Formation of β-phase hydride increases molar volume of Nb matrix by ~12 %, resulting in locally increased dislocation densities around hydride-Nb interface [38,39].

However, to clarify these possible mechanisms for the formation of planar boundaries in a single crystal of Nb, multiple batches of samples having similar slip system would need to be deformed in strategically chosen

orientations and would then need to be characterized by the same method, and identify the misorientation angle between cells using TEM diffraction analysis. The misorientation angle is a key parameter to understand the formation mechanism of LAGBs as well as homogeneity in mechanical deformation of a single grain. Heterogeneous deformation characteristics of single grain Nb has impeded efficient use of large grain Nb ingot slices to fabricate cavities; for example, bulging and irregularity of thickness after molding [15].

In the TEM study in Figure 6, attempts to measure the misorientation angle between dislocation cell blocks was hampered by the high angled wedge shape of the thin foils, which restricted the available range of tilt. Thus, further TEM investigation will be following as a future work in conjunction with multiple sample batch study.

4.2. FLUX PERTURBATION AT LAGBS

The MOI investigations show that magnetic flux preferentially penetrates both low and high angle grain boundaries, and coupling this with the observation of preferential precipitation of hydrides at the same boundaries suggests a link between the two. Although hydride precipitates are also distributed across the grain interiors (see Figure 7), they apparently did not have the same effect on flux-penetration as LAGBs in the MOI observation (see MO images in Figure 4 and Figure 5). Nb hydrides combined with dislocation networks locally reduce the superconducting order parameter and superconducting gap at LAGB, thereby leading to breakdown of superconductivity. Hydride precipitates at LAGBs also act as normal conductors to trap magnetic vortices while cooling down. Such trapped vortices are vibrated during RF operation of an SRF Nb cavity and this induces local heating. As a result, local thermal breakdown of RF superconductivity can occur on the surface [3,40]. In this study, cooling rate was constant across T_c of Nb ~9.2 K from the room temperature at a rate of 8-10 K/min, so there is probably no significant cooling rate related flux trapping effect on the MO imaging, as presented in Ref. 40.

Even though many of the hydride scars are large enough to be within spatial resolution limits in the MOI technique, the observed MO contrast is dominated by the collective influence of the defects at the boundaries (our previous MO studies show that this contrast requires close alignment between the applied magnetic field and the boundary plane [41]). LAGBs in this study seem to be not planar boundaries having small misorientation against external magnetic field, thus more detailed study is needed to clarify why only some of LAGBs are highly responsible for the magnetic flux perturbations. However, because MO imaging reflects more of a bulk than surface condition and the extensive hydride formation occurs primarily on the surface, this study suggests that nanometer size (< 100 nm) hydride segregation at grain boundaries [20, 21] can cause a similar magnetic flux disturbance, leading to GB weakness [41,42].

4.3. HYDRIDE DISTRIBUTION IN THE VICINITY OF LAGBS

EBSD micro-crystallographic analysis (see Figure 8) shows that a hydrogen depleted zone of ~20-60 μm width emerged on either side of the LAGBs after cryogenic cooling. The local average misorientation map suggests that a substantial amount of hydrogens migration toward the boundary occurred during the cooling. According to grain boundary segregation models in metal alloys [43, 44], GB segregation is known to be the result of dragging solute atoms to the GB in the form of vacancy-complexes. When plastic deformation is applied, non-equilibrium vacancy concentrations can be produced in the metal by dragging jogs in screw dislocations. The supersaturated vacancies can interact with hydrogen atoms and create supersaturated vacancy-solute complexes. The propensity of vacancies to sink to the GB gives rise to non-equilibrium grain boundary segregation with the solute atoms [27]. The schematic in Figure 10 illustrates a proposed mechanism of hydrogen transport to a LAGB due to vacancies: (a) at ambient condition, the equilibrium vacancy concentration exist in bulk Nb. (b) a tensile stress is applied, and the boundary is created by dislocation propagation and migration, with increased vacancy density. (c) with the boundary acting as a sink for vacancies, a non-equilibrium vacancy gradient and a concurrent transport of solute "H" atoms to the boundary occurs. (d) during cryogenic cooling, the H enriched complexes in the boundary preferentially nucleate hydrides at ~100-130 K. In this way, preferential hydride segregation at LAGB results from the vacancy sink. Romanenko [19] has previously described how hydride precipitation within top surface sheath of ~100 nm depth of a SRF Nb cavity can be

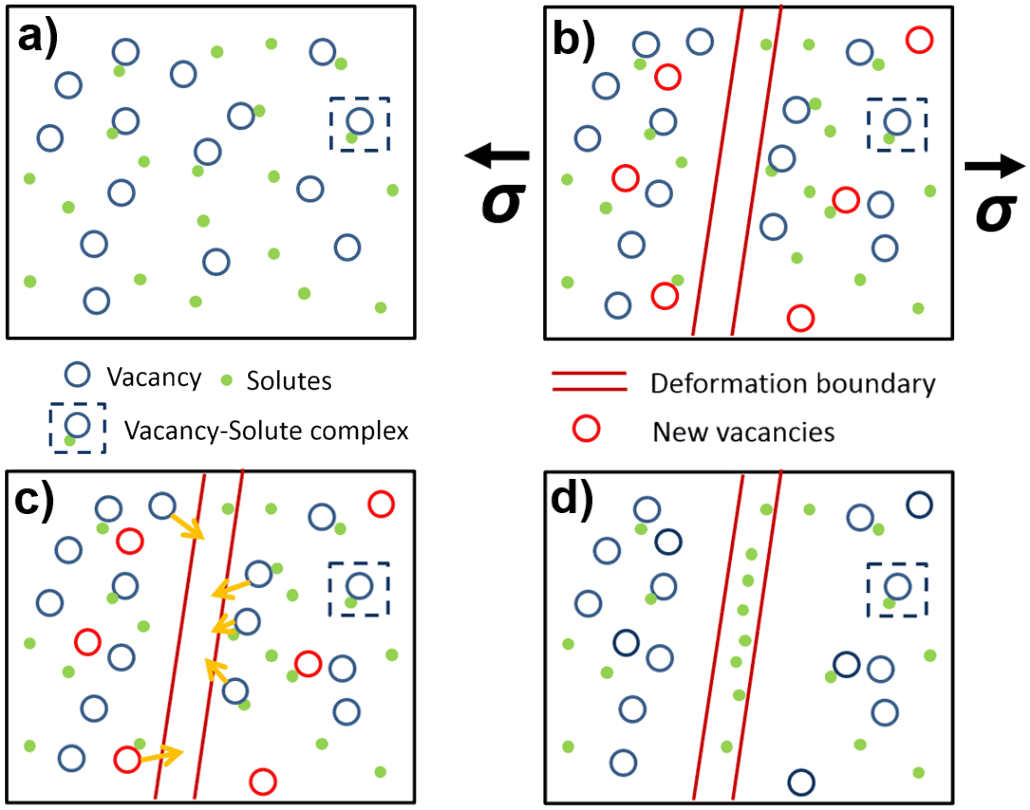

Figure 10. Schematic of $Nb_{1-x}H_x$ accumulation and precipitation at low angle grain boundaries (LAGBs) based on stressed induced non-equilibrium vacancies and their absorption into GB with concurrent transport of H to the boundary via vacancies [27,43, 44].

initiated from the formation of vacancy-H complexes, and the number of V-H complexes determine the density of hydride precipitates. Typical cooldown between 150 K and 2 K during SRF Nb cavity operation allows hydrogen atoms to diffuse up to a length of ~30 μm (L_{diff}), enabling segregation [22]. This diffusion distance is comparable to the width of the observed hydride depleted zone.

4.4. EFFECT OF 800°C ANNEAL

After the 800°C/2h anneal the pattern of flux penetration into the sample was substantially altered; while still suggesting some residual weakness at the LAGBs, the bulk properties are mostly recovered (see Figure 9). A plausible explanation is that residual hydrides at LAGBs beyond the resolution of MOI perturb the circulating superconducting currents and produce the very different magnetic flux penetration pattern that appear to be initiated from the surface. This surface initiated flux penetration has also been observed in a prior MO investigation [45] on a polycrystalline Nb coupon subjected to a series of surface treatments based on a previous cavity processing sequence (in that case, the 750°C anneal was followed by the + 120°C bake). The complicated treatments produced severe surface irregularity, so that flow of magnetic flux applied normal to the sample surface was significantly disturbed. However, the very shallow (few micrometer depth) of the surface groove at LAGB in this sample had much less severe topographic relief. The 800°C/2h anneal may be insufficient to remove all hydrogen atoms segregated at the LAGBs and the resulting formation of hydrides precipitated at LAGBs during cool-down may still locally degrade superconductivity; this would be consistent with a recent surface susceptibility study [46]. In this study, the 800°C heat treatment did not remove the very low angle boundaries which have a very low interfacial energy.

4.5. EFFECT OF CRYSTAL ORIENTATION

Although the mechanical deformation of the sample was designed to favor the production of a specific kind of

dislocation geometry, visual evidence of this effect on magnetic field penetration is suggested by the lesser amount of flux penetration in the "right" sample in Figure 4 and Figure 5. However, highly sensitive superconducting characterizations like AC susceptibility [46] or superconducting quantum interface device (SQUID) or vibrating sample magnetometer (VSM) [47] would be necessary to clearly understand the effect of dislocation structural morphology. These superconductivity characterizations require more specific sample preparation with a suitable size for measurements that would differ from current cavity processing techniques.

5. CONCLUSION

This study shows direct evidence of preferential hydride segregations at low angle grain boundaries (LAGBs) in SRF-grade high purity single crystal niobium through imaging of pits resulting from their decomposition. This segregated hydride phase correlates to a significant suppression of superconductivity at low angle grain boundaries produced by a low tensile strain (5%). These planar LAGBs were decorated with dense dislocations entanglements, since the tensile deformation was employed in parallel to the maximum shear stress. The low hydride concentration zone adjacent to the boundaries suggests that the LAGB segregation results from substantial "H" diffusion with the local non-equilibrium concentration of vacancy-H complexes. The MO imaging shows that 800 °C annealing process has a substantial effect on the magnetic flux perturbation of the sample but there is still some weakness of the LAGBs perhaps through a residual concentration of trapped H. Thus it is likely that higher temperature or longer thermal treatments would be required to completely eliminate the effect of the plastic deformation relative "H" contaminations in SRF-grade Nb. This is the first observation of cold work deformation induced superconducting degradation in SRF-grade Nb in terms of hydride precipitation and additional experiments are underway to study the effect of annealing temperature and nitrogen (N) and titanium (Ti) surface doping. While these results are relevant for large-grain cavities, similar phenomena probably occur in polycrystals, but it is not clear or easy to determine if the low angle boundaries within the grains affects hydride formation and flux trapping more than the plentiful high angle gain boundaries.

ACKNOWLEDGEMENT

This work was supported by the US DOE under awards DE-FG02-13ER41973 and DE-SC0009960 and by the State of Florida. The EBSD-OIM and HR TEM facilities at FSU are funded and supported by the Florida State University Research Foundation, and the National High Magnetic Field Laboratory, which is supported in part by the National Science Foundation Cooperative Agreement DMR-1157490.

REFERENCES

1. H. Padamsee, "RF Superconductivity vol II: Science, Technology and Application" (Weinheim: Wiley-VCH) (2009).
2. A. Yamamoto, M. Ross, N. Walker, "Advances in SRF development for ILC", in the proceedings of the 15th SRF workshop, Chicago, IL, USA, MOIOA02 (2011).
3. A. Gurevich, "Multiscale mechanisms of SRF breakdown", Physica C 441, pp. 38-43 (2006).
4. C. Z. Antoine, A. Aspart, J. P. Charrier, H. Safa, and B. Visentin, "Alternative approaches for surface treatment of Nb superconducting cavities" in the proceedings of the 9th SRF workshop, Santa Fe, USA, TAU008 (1999).
5. J. Knobloch, "The Q disease" in superconducting niobium RF cavities" AIP Conf. Proc., 671, pp.133-150 (2003).
6. C. Z. Antoine, B. Aune, B. Bonin, J. M. Cavedon, M. Juillard, A. Godin, C. Henriot, P. Leconte, H. Safa, A. Veyssiere, A. Chevarier, and B. Roux, "The role of atomic hydrogen in Q-degradation of niobium superconducting RF cavities: analytical point of view" in the proceedings of the 5th SRF workshop (DESY, Hamburg), pp.616-34, srf91f01 (1991).
7. A. Romanenko and H. Padamsee, "The role of near-surface dislocations in the high magnetic field performance of superconducting niobium cavities," Supercond. Sci. Technol., 23, 045008 (2010).
8. A. Romanenko, and L. V. Goncharova, "Elastic recoil detection studies of near-surface hydrogen in cavity-grade niobium" Supercond. Sci. Technol., 24, 105017 (2011).
9. J. Halbritter, "Transport in superconducting niobium films for radio frequency application", J. Appl. Phys., 97, 083904 (2005).
10. J. Halbritter, "On the oxidation and on the superconductivity of niobium", Appl. Phys. Solid Surface, 43, 1, pp. 1–28 (1987).
11. M. Delheusy, A. Stierle, N. Kasper, R. P. Kurta, A. Vlad,

H. Dosch, C. Antoine, A. Resta, E. Lundgren, and J. Andersen, "X-ray investigation of subsurface interstitial oxygen at Nb/oxide interfaces", Appl. Phys. Lett., 92, 101911 (2008).

12. G. Ciovati, "Improved oxygen diffusion model to explain the effect of low-temperature baking on high field losses in niobium superconducting cavities", Appl. Phys. Lett., 89, 022507 (2006).
13. T. Proslier, J. F. Zasadzinski, L. Cooley, C. Antoine, J. Moore, J. Norem, M. Pellin, and K. E. Gray, "Tunneling study of cavity grade Nb; Possible magnetic scattering at the surface", Appl. Phys. Lett., 92, 212505 (2008).
14. P. Kneisel, G. Ciovati, P. Dhakal, K. Saito, W. Singer, X. Singer, and G. R. Myneni, "Review of ingot niobium as a material for superconducting radio frequency accelerating cavities," Nucl. Instr. Meth. Phys. Res.: Accelerators, Spectrometers, Detectors and Associated Equipment, vol 774, pp.133-150 (2015).
15. T. R. Bieler, N. T. Wright, F Pourbohrat, C. Compton, K. T. Hartwig, D. Baars, A. Zamiri, S. Chandrasekaran, P. Darbandi, H. Jiang, E. Skoug, S. Balachandran, G. E. Ice, and W. Liu, "Physical and mechanical metallurgy of high purity Nb for accelerator cavities", Phys. Rev. ST Accel. Beams, 13, 031002 (2010).
16. R. J. Cava, B. Batlogg, J. J. Krajewski, H. F. Poulsen, P. Gammel, W. F. Peck, Jr., and L. W. Rupp, Jr., "Electrical and magnetic properties of $Nb_2O_{5-\delta}$ crystallographic shear structures, Phys. Rev. B, 44, 6973 (1991).
17. S. Isagawa, "Hydrogen absorption and its effect on low-temperature electric properties of niobium", J. Appl. Phys., 51, 8 (1980).
18. Barkov, A. Romanenko, and A. Grassellino, "Direct observation of hydrides formation in cavity-grade niobium", Phys. Rev. ST Accel. Beams, 15, 122001 (2012).
19. A. Romanenko, F. Barkov, L. D. Cooley, and A. Grassellino, "Proximity breakdown of hydrides in superconducting niobium cavities" Supercond. Sci. Technol., 26, 035003 (2013).
20. A. Romanenko, and L. V. Goncharova, "Elastic recoil detection studies of near-surface hydrogen in cavity-grade niobium" Supercond. Sci. Technol., 24, 105017 (2011).
21. A. Romanenko, C. J. Edwardson, P. G. Coleman, and P. J. Simpson, "The effect of vacancies on the microwave surface resistance of niobium revealed by positron annihilation spectroscopy", Appl. Phys. Lett., 102, 232601 (2013).
22. F. Barkov, A. Romanenko, Y. Trenikhina, and A. Grassellino, "Precipitation of hydrides in high purity niobium after different treatments", J. Appl. Phys., 114, 164904 (2013).
23. Y-J Kim, R Tao, R. F. Klie, and D. N. Seidman, "Direct atomic-scale imaging of hydrogen and oxygen interstitials in pure niobium using atom-probe tomography and aberration-corrected scanning transmission electron microscopy, ACS Nano,7(1), pp.732-739 (2012).
24. R. Tao, A. Romanenko, L. D. Cooley, and R. F. Klie, "Low temperature study of structural phase transitions in niobium hydrides" J. Appl. Phys., 114, 044306 (2013).
25. P. Maheshwari, F. A. Steviea, G. Myenenib, G. Ciovatib, J. M. Rigsbeec, and D. P. Griffisa, "Analysis of interstitial elements in niobium with secondary ion mass spectrometry (SIMS)", AIP Conf. Proc., 1352, 151 (2011).
26. Y. Trenikhina, A. Romanenko, J. Kwon, J-M. Zuo, and J. F. Zasadzinski, "Nanostructural features degrading the performance of superconducting radio frequency niobium cavities revealed by transmission electron microscopy and electron energy loss spectroscopy", J. Appl. Phys., 117, 154507 (2015).
27. X. Tingdong, "Creating and destroying vacancies in solids and non-equilibrium grain boundary segregation", Philos. Mag., 83, 7, pp.889-899 (2003).
28. D. Kuhlmann-Wilsdorf, and N Hansen, "Geometrically necessary, Incidental and Subgrain boundaries" Scripta Metallugica, 25, pp.1557-1562 (1991).
29. D. A. Hughes, N. Hasen, and D. J. Bammann, "Geometrically necessary boundaries, Incidental dislocation boundaries, and Geometrically necessary dislocations" Scripta Metallugica, 48, pp.147-153 (2003).
30. J. A. Rodrigues and R. Kirchheim, "More evidence for the formation of a dense Cottrell cloud of hydrogen (hydride) at dislocations in niobium and palladium", Scripta Metallurgica, 17, pp.159-164 (1983).
31. W. Singer, "SRF Cavity Fabrication and Material". arXiv preprint arXiv:1501.07142 (2015).
32. M. Wang, D. Kang, T.R. Bieler, C.C. Compton, Z. H. Sung, P. J. Lee, and A. A. Polyanskii, "Introduction of precisely controlled microstructural defects into SRF cavity niobium sheets and impact on local superconducting properties", in the proceedings of the 17th SRF workshop, MOPB018, Sep 13-18, Whistler, BC, Canada (2015).
33. D. Baars, PhD Dissertation, "Investigation of active slip systems in high purity single crystal niobium", Michigan

State University (2013).

34. A. A. Polyanskii, X. Y. Cai, D. M. Feldmann, and D. C. Larbalestier, "Visualization of magnetic flux in magnetic materials and high temperature superconductors uing the faraday effect in ferrimagnetic garnet films," in Nano-Crystalline and Thin Film Magnetic Oxides, I. Nedkov and M. Ausloos, Eds. Springer Netherlands, pp. 353-370 (1999).
35. R. Srinivansan, G. B. Viswanathan, V. I. Levit, and H. L. Fraser, "Orientation effect on recovery and recrystallization of cold rolled niobium single crystals" Mater. Sci. Eng. A, 507, pp. 179-189 (2009).
36. S. I. Wright, M. M. Nowell, D. P. Field, "A review of strain analysis using electron backscatter diffraction" Microsc. Microanal., 17, pp. 316-329 (2011).
37. D. Baars, H. Jiang, T. R. Bieler, A. Zamiri, F. Pourboghart, and C. Compoton, "Application of Texture Analysis: Ceramic Transactions (Wiley, New York) vol 201, p391 (2008).
38. C. Wainwright, A. J. Cook, and B. E. Hopkins, "The structures of niobium-hydride alloys", J Less-Common Met., 6, 362 (1964).
39. M. Amano ad Y. Sasaki, "Dislocation structure in dehydrogenated niobium" Phys. Status Solidi A, 19, 405 (1973).
40. S. Posen, M. Checchin, A. C. Crawford, A. Grassellino, M. Martinello, O. S. Melnychuk, A. Romanenko, D. A. Sergatskov, and Y. Trenikhina, "Efficient expulsion of magnetic flux in superconducting radiofrequency cavities for high Q0 applications", J. Appl. Phys., 119, 213903 (2016).
41. P. J. Lee, A. A. Polyanskii, A. Gurevich, A. A. Squitieri, D. C. Larbalestier, P. C. Bauer, C. Boffo, and H. T. Edwards, "Grain boundary flux penetration and resistivity in large grain niobium sheet," Physica C, vol 441, pp. 126-129 (2006).
42. Z-H Sung, PhD Dissertation, "The influence of grain boundaries on the properties of superconducting radio frequency cavity" University of Wisconsin – Madison (2010).
43. P. Lejček, "Grain boundary Segregation in Metals", Springer series in materials science (2010).
44. P. E. J. Flewitt and R. K. Wild, "Grain boundaries: Their Microstructure and Chemistry" (2001).
45. A. Polyanskii, P. Bauer, P. J. Lee, C. Boffo, L. Bellantoni, H. Edwards, A. Gurevich, M. Jewell, D. C. Larbalestier , G. K. Perkins, and A. Squitieri, "Inhomogeneous flux penetration in niobium sheet sampled across the cavity production route: An Investigation of the properties of BCP niobium for superconducting RF Cavities" in the proceedings of the 12th SRF workshop, TUP55, Ithaca, New York, USA (2005).
46. Z-H. Sung, A. Dzyuba, P. J. Lee, D. C. Larbalestier, and L. D. Cooley, "Evidence of incomplete annealing at 800°C and the effects of 120°C baking on the crystal orientation and the surface superconducting properties of cold-worked and chemically polished Nb," Supercond. Sci. Technol., 28, 075003 (2015).
47. S. B. Roy, G. R. Myneni, and V. C. Sahni, "On the reliable determination of the magnetic field for first flux-line penetration in technical niobium materials", Supercond. Sci. Technol. 21, 065002 (2008).